PHYSICAL REVIEW B **93**, 020104(R) (2016)

Titanium α-ω phase transformation pathway and a predicted metastable structure

N. A. Zarkevich[1,*] and D. D. Johnson[1,2,†]

[1]*Ames Laboratory, US Department of Energy, Ames, Iowa 50011-3020, USA*

[2]*Departments of Materials Science & Engineering and Physics, Iowa State University, Ames, Iowa 50011-2300, USA*

(Received 14 October 2015; revised manuscript received 15 December 2015; published 15 January 2016)

As titanium is a highly utilized metal for structural lightweighting, its phases, transformation pathways (transition states), and structures have scientific and industrial importance. Using a proper solid-state nudged elastic band method employing two climbing images combined with density functional theory DFT + U methods for accurate energetics, we detail the pressure-induced α (ductile) to ω (brittle) transformation at the coexistence pressure. We find two transition states along the minimal-enthalpy path and discover a metastable body-centered orthorhombic structure, with stable phonons, a lower density than the end-point phases, and decreasing stability with increasing pressure.

DOI: 10.1103/PhysRevB.93.020104

I. INTRODUCTION

Titanium is one of the four (Fe, Cu, Al, Ti) most used structural metals and is the key component of strong, lightweight structural alloys used in aerospace, military, and automotive applications. Mapping competing phases and the associated phase transformations with stress (or pressure, P), temperature (T), and impurities can provide predictive design for improved control of alloy properties, including stabilizing metastable transition structures. For Ti at hydrostatic pressures above 2 GPa, the ground-state hexagonal close-packed (hcp) α phase can transform into a brittle higher-density ω phase [1–3] (Fig. 1). At high P, Ti transforms to denser phases: $\alpha \rightarrow \omega \rightarrow \gamma \rightarrow \delta$ [4,5], while at high T it transforms to the body-centered cubic (bcc) β phase [6,7].

Previous theoretical investigations explored the transformation pathway—competing structures, minimum enthalpy pathway (MEP), and transition states (TSs)—and some key results are in conflict with observations. For example, from experimental data [1–6,8–15], the α-ω coexistence P_0 is 2 GPa, determined from the inequality $P_{\omega\rightarrow\alpha} < P_0 < P_{\alpha\rightarrow\omega}$ [16], valid for transformations between two solid anisotropic phases. At room temperature, the $\alpha \rightarrow \omega$ transition is observed between 2 and 15 GPa, depending on the pressure environment and sample purity. The $\omega \rightarrow \alpha$ transformation is observed below 2 GPa [9], but not for $P \geqslant 0$ for the pure hydrostatic case with a gas, methanol-ethanol, or argon medium [11]. Deviatoric anisotropic (uniaxial or shear) stress narrows the hysteresis [9,11]. The recent theoretical P_0 of 5.7 GPa [17] disagrees with experiment [9]. In addition, Ti has strongly correlated d electrons, and density functional theory (DFT) returns inaccurate relative enthalpies of the ground-state and competing structures (e.g., hcp is not the lowest-energy structure at 0 GPa), with a calculated $P_0 < 0$ between α and ω phases [18,19], which contradicts experiment [1–15].

Here we revisit the pressure-induced Ti α-ω transformation at the coexistence pressure. To detail the MEP and TSs, we use the generalized solid-state nudged elastic band (SS-NEB) method [20] based on DFT + U with on-site Hubbard corrections [21] to support the required accurate relative structural enthalpies, atomic forces, and stress tensor for unit cells used for SS-NEB [20]. Importantly, the SS-NEB method properly couples all atomic (or, using periodic unit cells, cell plus internal atomic) degrees of freedom and is mechanically consistent, including the MEP being invariant with cell size [20]. Adjusting $(U - J)$ to 2.2 eV in DFT + U, we correct the inaccurate relative enthalpies and obtain the observed hcp ground state at 0 GPa, and the observed coexistence pressure $P_0 = 2$ GPa; it is a value that reproduces the observed energy of reduction of Ti oxides (TiO_2 to Ti_2O_3), where 125 kJ/mol was matched by $(U - J) = 2.3 \pm 0.1$ eV [22].

Using SS-NEB combined with DFT + U, we find that the α-ω transformation has two TSs with a local enthalpy minimum, and discover a lower-density, body-centered orthorhombic (bco) metastable structure between them. This $\alpha \rightarrow$ bco $\rightarrow \omega$ transformation can be considered as a sequence of two transformations. Impurities, pressure, and temperature control the phase stability and transition barriers in most industrial and geophysical materials; in Ti, interstitial O, N, or C retard while substitutional Al and V suppress the ω phase [19]. The lower-density bco metastable TS structure might be stabilized by impurities or negative stresses—potentially induced by chemical interstitial or substitutional alloying.

II. METHODS

The α-ω transformation is considered in a 6-atom unit cell (Fig. 1). Applying the SS-NEB method [20], we detail the MEP (minimum enthalpy $H = E + PV$) and the transition states at coexistence pressure P_0 (Fig. 2), and versus applied pressures (Fig. 3). For accuracy, we use the SS-NEB method employing two climbing images (C2-NEB) [23,24], as tested on shape-memory transforms [25,26], to verify each TS. First, we turn off climbing and then sample the path by equidistant images. Next, one by one, each enthalpy maximum along the path is addressed by C2-NEB. We fully relax each local enthalpy minimum and verify its stability. The details of the structure, electronic density (Fig. 4), displacements, and stress components (Fig. 5) are also provided for completeness.

We employ DFT + U with on-site Hubbard corrections, [21] as implemented in VASP [27,28], using projector augmented waves (PAW) [29,30] and the PW91

*zarkev@ameslab.gov
†ddj@ameslab.gov

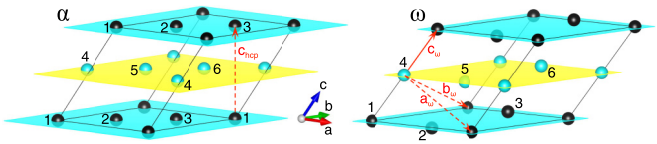

FIG. 1. Enumerated 6-atom unit cells of α (hcp) and ω structures, suitable for the TAO-1 α-ω transformation [18].

exchange-correlation functional [31]. For the 6-atom unit cell (Fig. 1), we use a 12^3 k-point mesh in the Brillouin zone, and a denser 24^3 k-mesh for the electronic density of states (DOS), see Fig. 6. Gaussian smearing with $\sigma = 0.05$ eV is used for relaxations; the tetrahedron method with Blöchl corrections [32] is used for the final total-energy calculations. Atomic structures and data [33] are visualized with VESTA [34] and GRACE software [35].

Phonons for the predicted bco structure are stable (Fig. 7); they are calculated via the small-displacement method [36]. Details are given in Sec. III.

III. RESULTS

Several mechanisms for the Ti α-ω transformation have been suggested [1–3,15,18]. Previous DFT results [18,19] found the ω phase to be the Ti ground state at 0 GPa. In contrast, using DFT + U [21] with $(U - J)$ adjusted to the experimental P_0 of 2 GPa—which matches the $(U - J)$ that also reproduces other Ti properties, such as the reduction energy of TiO_2—we obtained, not so surprisingly, the hcp α-Ti as the stable ground state at ambient pressure, in agreement with experiment.

From SS-NEB and C2-NEB calculations, we report the α-ω MEP at coexistence P_0 (Fig. 2), and MEP versus pressure (Fig. 3). Clearly, we find two TSs, and, in between, we find a

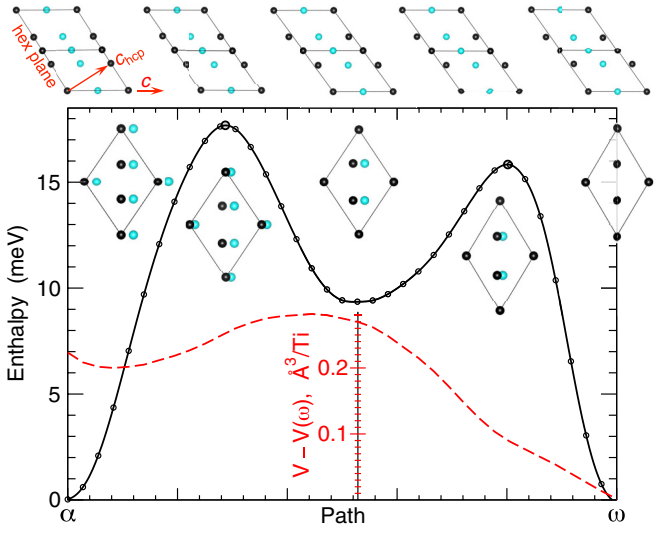

FIG. 2. Enthalpy (meV/atom) versus MEP at $P_0 = 2$ GPa, where α and ω enthalpies are equal within 0.15 meV/Ti. Dashed (red) line is volume V (Å^3/atom) relative to ω (central scale), where $V(\omega)$ is 17.55 Å^3/Ti. Atomic motion within a 6-atom cell is shown for hcp c axis (top): dark (black) circles and light (blue) circles indicate two hcp sublattices.

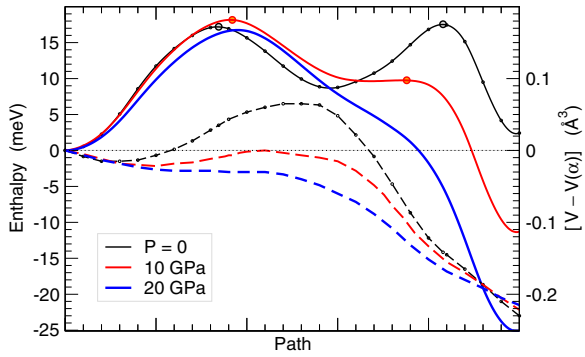

FIG. 3. From SS-NEB (lines) and C2-NEB (filled symbols), enthalpy (meV/atom) versus MEP at $P = 0$, 10, and 20 GPa. Change of volume (Å^3 per atom) relative to the α phase is given by dashed lines (right scale).

metastable intermediate structure (m), which is body-centered orthorhombic (bco). Hence, the α-ω MEP consists of α-m and m-ω transformations, with two barriers along the α-m-ω path (18 meV and 16 meV, respectively). Recall that each nudged image in the SS-NEB attempts to be equidistant from its neighbors along the MEP, and minimizes its enthalpy in all other directions within the NEB code [20,23,37]. Hence, an enthalpy minimum along the MEP must be a local enthalpy minimum, i.e., a stable or metastable structure. Indeed, being fully relaxed, the local enthalpy minimum m (Fig. 4) does not transform to another structure, and, as expected, it has a stable phonon spectrum (Fig. 7). At low pressures, this bco structure has a lower density than the α phase, see volume in Figs. 2 and 3, and might be stabilized by dopants or negative stress.

While a new metastable bco structure is found, the MEP is still the TAO-1 ("saloon-door" transition) path discussed by Trinkle *et al.* [18]. Other paths, including the α-bcc-ω, suggested by Usikov [2] and ruled out by later experiments [11], have substantially higher enthalpy barriers, in agreement with the previous calculations [18].

At each pressure, we find two barriers in *energy* E for the α-ω transformation. However, due to volume decrease along the MEP, the second barrier in *enthalpy* $H = E + PV$ is suppressed at $P > 10$ GPa, see Fig. 3, so the stability of the bco structure decreases with pressure. In principle, this metastable intermediate structure during the α-ω transformation can be

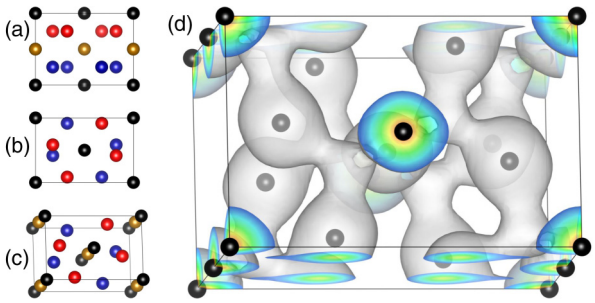

FIG. 4. 12-atom (conventional) unit cell of the metastable bco structure with layers of atoms (left), projected along a (a), b (b), and viewed approximately along b (c,d), where $a < b < c$. (d) Isosurfaces of electronic density (0.033 e^-/Å^3).

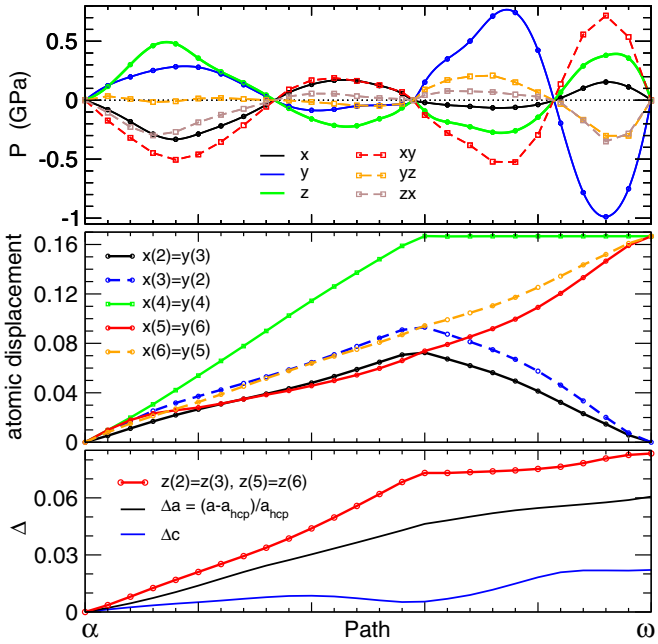

FIG. 5. Diagonal P_i and off-diagonal P_{ij} stress components (GPa), absolute values of the atomic displacements (x,y,z) in direct lattice coordinates (dimensionless), with atom 1 fixed at (0,0,0), and elongation Δ (dimensionless) of the lattice translation vectors a and c (relative to the hcp α phase) in the 6-atom cell (Fig. 1 and Fig. 2 insets) versus MEP at zero pressure.

determined experimentally by x-ray diffraction (XRD), as this process might be too fast for neutron scattering.

Note that the transformation generates significant anisotropic stress (Fig. 5). On the other hand, pressure anisotropy can facilitate the transformation. Indeed, an applied uniaxial or shear stress narrows the hysteresis in experiment [9,11]. In fact, the reverse $\omega \rightarrow \alpha$ transformation does not happen at $P \geqslant 0$ under hydrostatic conditions. As expected, anisotropic stress disappears at every equilibrium point, either stable (α, m, and ω structures) or unstable (both TSs); see Fig. 5. During the transformation at P_0, the electronic DOS has a minimum near the Fermi energy, E_F, for α, m, and ω

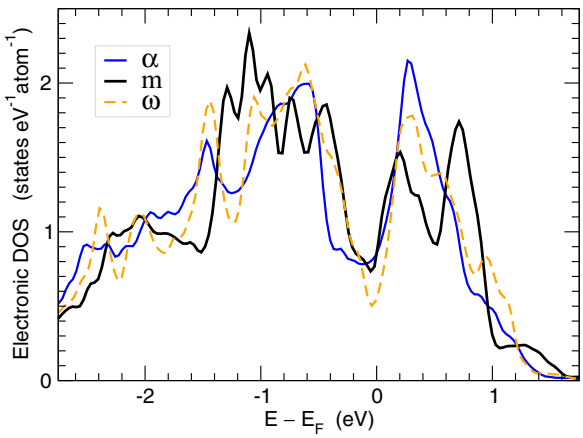

FIG. 6. DOS versus energy E (relative to E_F) for Ti α, m, and ω phases at 2 GPa, with local minima at E_F.

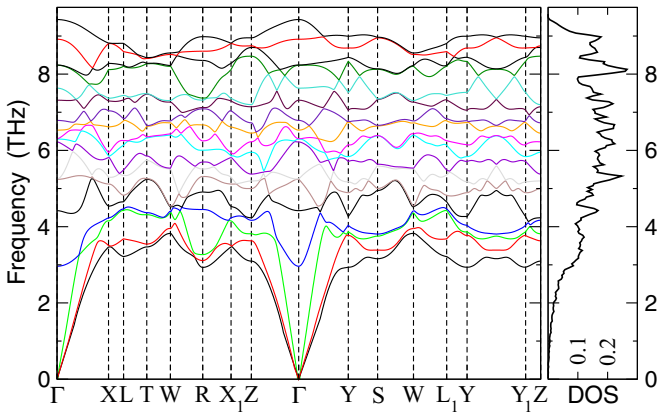

FIG. 7. Phonon frequencies and DOS in the metastable bco structure at 2 GPa (coexistence pressure).

structures (Fig. 6), as well as both TS configurations, which are the saddle points on the potential enthalpy hypersurface.

A. Phonons of the metastable bco structure

Phonons for the predicted bco structure are calculated via the small-displacement method, using the PHON code [36]. At the α-ω coexistence pressure (2 GPa), we displace each of the 6 atoms by 0.04 Å in three directions in the 162-atom $3 \times 3 \times 3$ supercell of the bco cell. The calculated atomic forces (with subtracted forces of the relaxed structure) are used to construct the force-constant matrix, symmetrized for bco. The titanium atomic mass is 47.867 a.u. The phonon DOS is calculated with 0.05 THz smearing and 21^3 k-point mesh.

The accompanying file FORCES [38] provides the calculated atomic forces for each of the 18 displacements (by 0.0025 T_i along each vector T_i, $i = 1,2,3$) of 6 atoms in the primitive unit cell (atoms 1, 28, 55, 82, 109, and 136 in the 162-atom $3 \times 3 \times 3$ supercell, file POSCAR [38]).

B. Structural properties

The calculated structural parameters are given in Tables I and II. As expected, a positive Hubbard correction in DFT + U [21] adds repulsion between electrons on the same d orbital, which results in a slight increase of the lattice constants (which are 1% larger than in experiment) and atomic volume V_0, reported together with the bulk modulus B_0 and its pressure

TABLE I. Direct coordinates of Ti atoms in the bco structure in terms of the translation vectors of the primitive 6-atom unit cell, $T_1 = (-a/2,b/2,c/2)$; $T_2 = (a/2,-b/2,c/2)$; $T_3 = (a/2, b/2,-c/2)$, where the orthogonal lattice vectors at 2 GPa are $a = 5.02$; $b = 5.58$; $c = 7.63$ Å.

0	0	0
0.573337942	0.239952296	0.166666667
0.426652476	0.593264863	0.666666667
0.5	0	0.5
0.073340952	0.406758964	0.833333333
0.926655948	0.760071300	0.333333333

TABLE II. Lattice constants (Å) at 0 GPa and Birch-Murnaghan parameters V_0 (Å^3/atom), B_0 (GPa), and B_0' of the α, ω, and m phases from DFT + U, neutron diffraction, [41], and compressibility measurements [42].

	a, b	c (Å)	V_0	B_0	B_0'	Method
α	2.972	4.728	18.09	111.7	3.6	DFT + U
	2.9506(2)	4.6795(4)	17.64	109.353	3.355	Expt.
ω	4.656	2.854	17.86	112.9	3.4	DFT + U
	4.614(1)	2.832(1)	17.4			Expt.
m	5.052, 5.613	7.676	18.15	109.2	3.3	DFT + U

derivative B_0' in Table II. These parameters were obtained by the least-squares fit of the Birch-Murnaghan equation of state to calculated volumes of the relaxed structures at hydrostatic pressure. The accuracy of the DFT + U methodology is well discussed in the literature [22,39,40].

IV. SUMMARY

We have detailed the pressure-induced Ti α-ω transformation at the coexistence pressure via combined DFT + U [21] and SS-NEB methods [20,23], using two climbing images in C2-NEB [23] for multiple transition states. With a judicious choice of $(U - J) = 2.2$ eV, DFT + U [21] reproduces the observed coexistence pressure ($P_0 = 2$ GPa) and the ground state (α at $P < 2$ GPa) and provides correct relative structural enthalpies. It is not fortuitous that the same choice also reproduces well the reduction energies of Ti oxides [22]. Importantly, we found a metastable body-centered orthorhombic (bco) structure between two transition states (enthalpy barriers) along the minimal-enthalpy path. The predicted structure has stable phonons and a lower density than the α and ω end-point phases, but it has decreasing stability with increasing pressure (it is not stable above 10 GPa); it might be stabilized by impurities (under investigation), and provides an opportunity for engineering of lower-density titanium alloys, with additional strengthening by precipitation.

ACKNOWLEDGMENTS

This work was supported by the US Department of Energy (DOE), Office of Science, Basic Energy Sciences, Materials Science and Engineering Division. The research was performed at the Ames Laboratory, which is operated for the US DOE by Iowa State University under Contract No. DE-AC02-07CH11358.

[1] J. M. Silcock, Acta Metall. **6**, 481 (1958).
[2] M. P. Usikov and V. A. Zilbershtein, Phys. Status Solidi A **19**, 53 (1973).
[3] A. Rabinkln, M. Tallanker, and O. Botstein, Acta Metall. **29**, 691 (1981).
[4] Y. K. Vohra and P. T. Spencer, Phys. Rev. Lett. **86**, 3068 (2001).
[5] Y. Akahama, H. Kawamura, and T. Le Bihan, Phys. Rev. Lett. **87**, 275503 (2001).
[6] A. Jayaraman, W. Klement, and G. C. Kennedy, Phys. Rev. **131**, 644 (1963).
[7] J. C. Jamieson, Science **140**, 72 (1963).
[8] V. A. Zilbershteyn, G. I. Nosova, and E. I. Estrin, Fiz. Met. Metalloved. **35**, 584 (1973).
[9] V. A. Zilbershteyn, N. P. Chistotina, A. A. Zharov, N. S. Grishina, and E. I. Estrin, Fiz. Met. Metalloved. **39**, 445 (1975).
[10] E. Yu. Tonkov, *High Pressure Phase Transformations: A Handbook*, Vol. 2 (Gordon and Breach Science, Philadelphia, 1992).
[11] D. Errandonea, Y. Meng, M. Somayazulu, and D. Häusermann, Physica B (Amsterdam) **355**, 116 (2005).
[12] Y. Vohra, S. Sikka, S. Vaidya, and R. Chidambaram, J. Phys. Chem. Solids **38**, 1293 (1977).
[13] L. C. Ming, M. Manghnani, and M. Katahara, Acta Metall. **29**, 479 (1981).
[14] C. W. Greeff, D. R. Trinkle, and R. C. Albers, J. Appl. Phys. **90**, 2221 (2001).
[15] N. Adachi, Y. Todaka, H. Suzuki, and M. Umemoto, Scr. Mater. **98**, 1 (2015).
[16] N. A. Zarkevich and D. D. Johnson, Phys. Rev. B **91**, 174104 (2015).
[17] J. Zhang, Y. Zhao, R. S. Hixson, G. T. Gray III, L. Wang, W. Utsumi, S. Hiroyuki, and H. Takanori, J. Phys. Chem. Solids **69**, 2559 (2008).
[18] D. R. Trinkle, R. G. Hennig, S. G. Srinivasan, D. M. Hatch, M. D. Jones, H. T. Stokes, R. C. Albers, and J. W. Wilkins, Phys. Rev. Lett. **91**, 025701 (2003).
[19] R. G. Hennig, D. R. Trinkle, J. Bouchet, S. G. Srinivasan, R. C. Albers, and J. W. Wilkins, Nat. Mater. **4**, 129 (2005).
[20] D. Sheppard, P. H. Xiao, W. Chemelewski, D. D. Johnson, and G. Henkelman, J. Chem. Phys. **136**, 074103 (2012).
[21] S. L. Dudarev, G. A. Botton, S. Y. Savrasov, C. J. Humphreys, and A. P. Sutton, Phys. Rev. B **57**, 1505 (1998).
[22] S. Lutfalla, V. Shapovalov, and A. T. Bell, J. Chem. Theory Comput. **7**, 2218 (2011).
[23] N. A. Zarkevich and D. D. Johnson, J. Chem. Phys. **142**, 024106 (2015).
[24] N. A. Zarkevich and D. D. Johnson, C2NEB source code, http://lib.dr.iastate.edu/ameslab_software/1.
[25] N. A. Zarkevich and D. D. Johnson, Phys. Rev. Lett. **113**, 265701 (2014).
[26] N. A. Zarkevich and D. D. Johnson, Phys. Rev. B **90**, 060102 (2014).
[27] G. Kresse and J. Hafner, Phys. Rev. B **47**, 558(R) (1993).
[28] G. Kresse and J. Hafner, Phys. Rev. B **49**, 14251 (1994).
[29] P. E. Blöchl, Phys. Rev. B **50**, 17953 (1994).
[30] G. Kresse and D. Joubert, Phys. Rev. B **59**, 1758 (1999).
[31] J. P. Perdew, J. A. Chevary, S. H. Vosko, K. A. Jackson, M. R. Pederson, D. J. Singh, and C. Fiolhais, Phys. Rev. B **46**, 6671 (1992); **48**, 4978 (1993).
[32] P. E. Blöchl, Phys. Rev. B **62**, 6158 (2000).
[33] N. A. Zarkevich, Complexity **11**, 36 (2006).

[34] K. Momma and F. Izumi, J. Appl. Crystallogr. **44**, 1272 (2011).
[35] E. Stambulchik, Grace Development Team, Grace software, http://plasma-gate.weizmann.ac.il/Grace.
[36] D. Alfè, Comput. Phys. Commun. **180**, 2622 (2009).
[37] H. Jónsson, G. Mills, and K. W. Jacobsen, in *Classical and Quantum Dynamics in Condensed Phase Simulations*, Proceedings of the International School of Physics (Villa Narigola, Lerici, Italy), edited by B. J. Berne, G. Ciccotti, and D. F. Coker (World Scientific, Singapore, 1998), p. 385.
[38] See Supplemental Material at http://link.aps.org/supplemental/10.1103/PhysRevB.93.020104 for accompanying files FORCES and POSCAR.
[39] C. Loschen, J. Carrasco, K. M. Neyman, and F. Illas, Phys. Rev. B **75**, 035115 (2007).
[40] N. J. Mosey and E. A. Carter, Phys. Rev. B **76**, 155123 (2007).
[41] G. T. Gray III, C. E. Morris, and A. C. Lawson, in *Titanium'92, Science and Technology: Proceedings of the 7th International Conference on Titanium (San Diego, California)*, Sponsored by the Titanium Committee of the Minerals, Metals & Materials Society, edited by F. H. Froes and I. L. Caplan (Minerals, Metals, and Materials Society, Warrendale, PA, 1992), Vol. 1, pp. 225–232.
[42] S. N. Vaidya and G. C. Kennedy, J. Phys. Chem. Solids **33**, 1377 (1972).